# Graph-Guided Adaptive Formation Control with Prescribed Performance Enhanced by Neural Network-Based Backstepping

Fengxi Xie , Guozhen Liang , Ying-Ren Chien *

Posted Date: 29 February 2024

doi: 10.20944/preprints202402.1744.v1

Keywords: Autonomous vehicle; trajectory tracking; formation control; prescribed performance

 doi:10.20944/preprints202402.1744.v1



*Article*

# Graph-Guided Adaptive Formation Control with Prescribed Performance Enhanced by Neural Network-Based Backstepping

**Fengxi Xie [1,†], Guozhen Liang [1,†], and Ying-Ren Chien[2,*]**

[1] Department of Electrical engineering and computer science, Technische Universität Berlin, 10623 Berlin, Germany
[2] Department of Electrical Engineering, National Ilan University, Yilan 26047, Taiwan
* Correspondence: yrchien@niu.edu.tw
† These authors contributed equally to this work.

**Abstract:** This research addresses the formidable challenge of achieving precise trajectory tracking for autonomous vehicle formations in uncertain environments. It introduces an adaptive control system tailored for autonomous vehicles, with a primary focus on ensuring prescribed performance in trajectory tracking within a leader-follower formation paradigm. The system incorporates a guidance law that allows the leader vehicle to dynamically adjust desired yaw angles and speeds for follower vehicles based on the established reference trajectory, enhancing tracking accuracy and responsiveness to environmental changes. To address practical external disturbances, the study utilizes Radial Basis Function Neural Networks (RBFNN) in conjunction with second-order filters for error approximation. This approach is further strengthened by a carefully formulated adaptive law. The innovative integration of a barrier Lyapunov function with the backstepping method significantly enhances the system's adaptability and robustness, ensuring trajectory tracking performance meets predetermined standards. Simulation results illustrate the control system's adept handling of various external disturbances, consistently maintaining trajectory tracking errors within predefined limits. This underscores the system's potential to markedly enhance the operational reliability and efficiency of autonomous vehicle formations in unpredictable environmental conditions.

**Keywords:** autonomous vehicle; trajectory tracking; formation control; prescribed performance

## 1. Introduction

The coordination of multi-autonomous vehicles has become a significant area of research, with a focus on diverse formation control strategies, including behavior-based control [1], virtual structure [2], and decentralized control [3]. Behavior-based formation control emphasizes local interactions among vehicles to form desired patterns, while virtual structure formation control guides the vehicles to maintain their relative positions within an invisible geometric framework. In decentralized control, individual vehicles make decisions based on local information and communication with neighbors. Despite the advantages of these approaches, this paper will investigate leader-follower formation control for multi-autonomous vehicles. This method has been selected due to its simplicity, ease of implementation, and the potential for achieving robust performance under specific conditions [4–6].

There has been a significant amount of research conducted on the subject, and a considerable portion of it is of high quality. Yang and Gu et al. [7] realized a non-linear formation keeping and mooring control of multiple autonomous underwater vehicles by combining Lyapunov's direct method with a smooth feedback control law. A leader-follower framework is utilized to develop a guided formation control scheme through a modular design procedure, drawing inspiration from integrator backstepping and cascade theory concepts [8]. In order to mitigate the negative effects caused by communication delays, a control system that can effectively manage inter-vehicle communication issues is designed [9], which can be particularly challenging in underwater environments. Also, Yan et al. [10] present coordinated control protocols, both with and without time delay, to address the

 doi:10.20944/preprints202402.1744.v1



coordination control problem of multiple Autonomous Underwater Vehicles (AUVs) under switching communication topologies using discrete information.

To design stable controllers, many methods are used, among which the sliding mode control (SMC) method is quite popular. SMC is a robust control method that can effectively suppress the effects of external disturbances and modeling uncertainties, making it well-suited for applications with non-linear and uncertain dynamics [11–14]. Wu et al. [12] combine SMC and backstepping techniques to design a closed-loop control system to deal with uncertainty in formation control and demonstrate the effectiveness of the method. Wang et al. [13] proposed a new method to deal with the uncertainties. The approach involves utilizing sliding mode control, multilayer neural networks, and adaptive robust techniques to design an effective formation controller for underwater vehicles. Also, Su et al. [15] built an adaptive fixed time integral sliding mode disturbance observer to accurately estimate compound disturbance. Nevertheless, the use of sliding mode control (SMC) comes with a notable disadvantage known as chattering [16]. To address this issue and enhance the system's robustness, various methods have been introduced. Backstepping method is one of them. Backstepping control offers a systematic and recursive approach to designing control laws for complex nonlinear systems, ensuring stability and providing flexibility in handling uncertainties and disturbances, making it an advantageous choice compared to sliding mode control [17–19]. The Lyapunov-based backstepping approach is developed and proved to be able to work effectively [17,18]. Also, Wang et al. [20] built a graphtheory-based backstepping controller to deal with the disturbance. Zaidi et al. [21] developed a combined approach of chatter-free sliding mode control and backstepping technique in their design. Yang et al. [22] presented a controller that combines backstepping and sliding mode control techniques to effectively address external disturbances. Also, neural networks have gained popularity in recent years for handling uncertainty disturbances [23–25]. Neural networks possess the property of universal function approximation, enabling them to approximate any continuously differentiable function. Using RBFNN to deal with the uncertainties is proved very efficient [26,27]. Using RBFNN and combining LKFs and backstepping techniques, Zhao et al. [28] proposed a control scheme. Besides, guidance laws are widely utilized in trajectory tracking problems. They can effectively improve the robustness and adaptive performance of the system [29–31]. Incorporating guidance laws into formation control is a beneficial approach to consider.

However, achieving a stable performance of the system is challenging, despite the inherent difficulty in maintaining stable system performance, a breakthrough was first made with the development of the prescribed performance control (PPC) method. The core concept of achieving predefined transient and steady-state performance of output tracking error is captured by an innovative PPC approach introduced in [32], employing a transformation function that strictly increases or decreases the tracking error. Recently, more PPC methods have been developed [22,33–35]. They have achieved good results, but the challenge for formation control remains [36]. Mehdifar et al. [37] presented a graph-based formation control approach for leader-follower multiagent systems in a distributed manner using a prescribed performance strategy, yielding favorable outcomes. However, the method does not account for external disturbances. Dai et al. [36] incorporates barrier Lyapunov functions and an adaptive backstepping procedure to ensure the boundedness of the closed-loop systems while guaranteeing transient performance. However, their method heavily relies on the accuracy of dynamic modeling, which implies that its robustness and adaptive may be limited. Jiang et al. [35] suggests a prescribed-time formation control approach for second-order nonlinear multi-agent systems with a directed graph. However, there is room for further optimization of the system responsiveness of this approach. In a word, the formation members have limited communication capabilities, and complex algorithms may hinder the controller's performance. Additionally, accurately approximating disturbances is challenging, which can impact the system's robustness and adaptability [6,38,39].

In this paper, a controller is proposed for autonomous vehicle formation control, combining the leader-follower method and backstepping technique. The leader's predefined trajectory and desired

 doi:10.20944/preprints202402.1744.v1



formation shape guide the generation of desired yaw angles and velocities for the followers using a graph-based guidance law. Nonlinear error handling is achieved through a second-order filter and RBFNN, complemented by an adaptive law. Furthermore, a barrier Lyapunov function is employed to achieve prescribed performance control. In comparison with previously mentioned methods, our main contributions can be summarized as follows: (1) This work combines these approaches, enabling precise trajectory tracking and formation maintenance in autonomous vehicle formation control. (2) The graph-based guidance law generates desired yaw angles and velocities based on the formation members' graph relationship, ensuring accurate formation control and alignment with the leader's trajectory. (3) The use of second-order filters and RBFNN effectively handles nonlinear errors, improving control performance by mitigating non-linearities, enhancing stability, and tracking accuracy. The adaptive law further enhances adaptability to changing dynamics.

The rest of this paper is structured as follows: In Section 2, we introduce the vehicle's kinetic and dynamic model. Section 3 describes the design of the proposed controller, where we employ a Lyapunov function to demonstrate stability. Section 4 presents the simulation results for formation trajectory tracking control in the presence of external disturbances. Finally, Section 5 conclues this work.

## 2. Kinematics and Dynamics Models

Referring to Figure 1, the kinematics and dynamics of the vehicle is

$$\begin{cases} \dot{x}_i = v_i \cos(\theta_i) \\ \dot{y}_i = v_i \sin(\theta_i) \\ \dot{\theta}_i = \sigma_i^{-1} v_i \tan(\delta_i) + f_{\theta,i}(\theta_i) + d_{\theta,i} \\ \dot{v}_i = F_i + f_{v,i}(v_i) + d_{v,i} \end{cases} \tag{1}$$

where the constant $\sigma_i > 0$ is the length of each vehicle. Here, $(x_i, y_i)$ is the reference point of the vehicle with $i \in \{1, \ldots, n\}$ and is placed at the midpoint of the rear axle, with $x_i \in \mathbb{R}$ being the longitudinal position and $y_i \in (-a, a)$ being the lateral position of the vehicle in an inertial frame with Cartesian coordinates $(X, Y)$; $v_i$ is the speed of the vehicle at the point $(x_i, y_i)$, $\theta_i \in \left(-\frac{\pi}{2}, \frac{\pi}{2}\right)$ is the angular orientation of the vehicle with respect to the $X$ axis, $\delta_i$ is the steering angle of the front wheels relative to the orientation $\theta_i$ of the vehicle, and $F_i$ is the acceleration of the vehicle. $f_{\theta,i}(\theta_i)$ and $f_{v,i}(v_i)$ are unknown nonlinear functions. $d_{\theta,i}(t)$ and $d_{v,i}(t)$ denote unknown and bounded external disturbances.

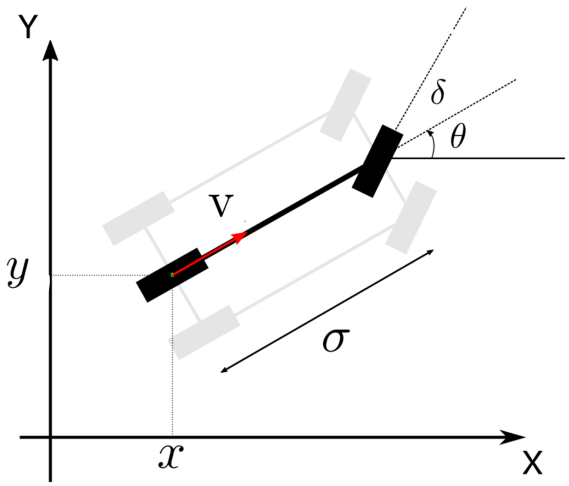


**Figure 1.** Vehicle Model

 doi:10.20944/preprints202402.1744.v1



**Lemma 1.** *Nonlinear function* $\boldsymbol{g(x)}$ *can be approximated by an RBFNN under given accuracy* $\bar{\varepsilon} > 0$. *That is,* $\boldsymbol{g(x)}$ *can be written as*

$$\boldsymbol{g(x)} = \boldsymbol{W}^T \boldsymbol{\varphi(x)} + \varepsilon(\boldsymbol{x}),$$

*where* $W \in R^l$ *is the ideal constant weight vector,* $\varepsilon(\boldsymbol{x})$ *is the approximation error satisfying* $|\varepsilon(\boldsymbol{x})| \leq \bar{\varepsilon}.\boldsymbol{\varphi(x)} = (\varphi_1(\boldsymbol{x}), \varphi_2(\boldsymbol{x}), \ldots, \varphi_l(\boldsymbol{x}))^T$ *denotes the Gaussian basis function vector with* $\varphi_j(\boldsymbol{x}) = \exp\left(-\frac{\|\boldsymbol{x}-\varrho\|^2}{2\sigma^2}\right), j = 1, 2, \ldots, l$, *where* $\varrho$ *and* $\sigma$ *are the center and width of Gaussian basis function* $\varphi_j(\boldsymbol{x})$, *respectively.* $\boldsymbol{x} = (x_1, x_2, \ldots, x_q)^T$. *Then we have* $\|\boldsymbol{\varphi(x)}\|^2 \leq \|\boldsymbol{\varphi(\dot{x})}\|^2$, *where* $\dot{\boldsymbol{x}} = (x_1, x_2, \ldots, x_r)^T, r \leq q$.

**Lemma 2.** *For* $\forall a, b \geq 0$, *and* $p, q > 0$, *satisfying* $1/p + 1/q = 1$, *the inequality holds as* $ab \leq \frac{a^p}{p} + \frac{b^q}{q}$.

## 3. Controller Design

In this section, we propose a formation tracking controller for the vehicle formation members. Figures 2 and 3 illustrate the setup, where member $i$ follows leader $j$ as its follower. The whole system is designed with the help of backstepping technique. The leader's desired trajectory is given, and based on the leader's kinematics and dynamics, its desired velocity and steering angle are designed and fed into the guidance law. Subsequently, we calculate the desired yaw angle $\theta_{d,i}$ and velocity $v_{d,i}$ for the followers, which are then used as inputs to their respective steering angle and velocity controllers. To ensure high robustness against unknown disturbances, we employ a second-order filter to estimate the error and use a Radial Basis Function Neural Network (RBFNN) to approximate the unknown non-linear function. For this purpose, we design an adaptive law. Additionally, we consider a nominal function in the system and introduce another adaptive law to handle it. Finally, we compute the final desired steering angle and velocity to guide the followers effectively.

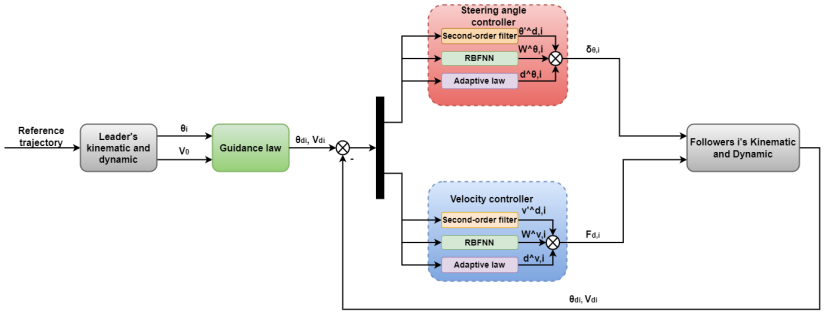


**Figure 2.** Formation controller diagram

 doi:10.20944/preprints202402.1744.v1



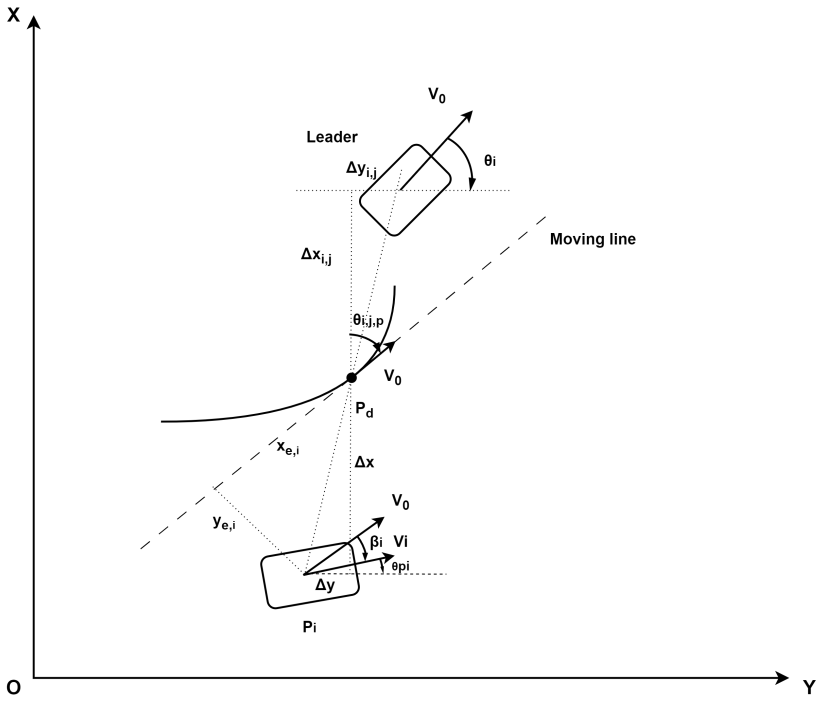


**Figure 3.** formation control geometric relationship

### *3.1. Guidance Law Design*

The guidance law is specifically designed to enhance the system's flexibility and adaptability. In this context, the formation's desired shape is predefined, while the initial positions of the formation members are randomized. To illustrate, let's consider the scenario involving a leader (denoted as $j$) and one of its followers ($i$). The current position of follower $i$ is represented as $p_i$, while $p_{i,d}$ signifies its desired position. The desired position vector $\boldsymbol{p}_{i,d} = [x_{i,d}, y_{i,d}]^{\mathrm{T}} = [x_i, y_i]^{\mathrm{T}} + [\Delta x, \Delta y]^{\mathrm{T}}$.

Based on Figure 3, our objective is to control member $i$ effectively, which involves ensuring that $p_i$ converges to the desired position. We define an error term to achieve this and aim to drive it to convergence. This error is described as (2).

$$\begin{bmatrix} x_{e,i} \\ y_{e,i} \end{bmatrix} = \begin{bmatrix} \cos\theta_{i,j,p} & -\sin\theta_{i,j,p} \\ \sin\theta_{i,j,p} & \cos\theta_{i,j,p} \end{bmatrix}^{T} \left( \boldsymbol{p}_i - \boldsymbol{p}_{i,d} \right) \tag{2}$$

where $\theta_{i,j,p} = \operatorname{atan2}\left(y_i'(t) + \Delta y'(t), x_i' + \Delta x'\right) \in [-\pi, \pi]$, $y_{e,i}$ is the shortest distance between the real position $\boldsymbol{p}_i$ of the vehicle $i$ and the moving line of the desired position $\boldsymbol{p}_{i,d}$, $x_{e,i}$ is the distance along the moving line between the real position $\boldsymbol{p}_i$ of the vehicle $i$ and the moving line of the desired position $\boldsymbol{p}_{i,d}$.

To minimize the error and approach zero, it is essential to calculate the error precisely. We can easily obtain the derivative of $y_{e,i}$ as follows:

$$\dot{y}_{e,i} = v_i \sin\left(\theta_i - \theta_{p,i}\right). \tag{3}$$

The barrier Lyapunov function is employed in the design of the governing law to restrict the error and ensure the controlled member maintains a stable state during motion. Moreover, separate Lyapunov candidates are designed for $y_{e,i}$ and $x_{e,i}$ to significantly reduce interference between different errors. A Lyapunov function for $y_{e,i}$ is presented as follows:

$$V_1 = \frac{b_{y,i}^2}{\pi} \tan\left(\frac{\pi {y_{e,i}}^2}{2b_{y,i}^2}\right), \tag{4}$$

 doi:10.20944/preprints202402.1744.v1



where $b_{y,i}$ is the upper boundary of $y_{e,i}$.

By taking the derivative of Eq. (4), one can prove the stability of $V_1$ as follows:

$$\dot{V}_1 = \frac{y_{e,i}\dot{y_{e,i}}}{\cos^2\left(\frac{\pi {y_{e,i}}^2}{2b_{y,i}^2}\right)} + \frac{2b_{y,i}\dot{b}_{y,i}}{\pi}\tan\left(\frac{\pi {y_{e,i}}^2}{2b_{y,i}^2}\right) - \left(\frac{\dot{b}_{y,i}}{b_{y,i}}\right)\frac{{y_{e,i}}^2}{\cos^2\left(\frac{\pi {y_{e,i}}^2}{2b_{y,i}^2}\right)}. \tag{5}$$

Based on the vector field guidance law, the desired yaw angle $\theta_{d,i}$ is designed as follows:

$$\theta_{d,i} = \theta_{p,i} + \arcsin\left(-\frac{k_y b_{y,i}^2}{2v_i \pi y_{e,i}}\sin\left(\frac{\pi y_{e,i}^2}{b_{y,i}^2}\right) + \frac{\dot{b}_{y,i}}{v_i b_{y,i}} y_{e,i}\right), \tag{6}$$

where $k_y > 0$ is the guidance law parameter, which is used to represent the strength of the vector field.

Defining $k_b = \sup\left|\frac{\dot{b}_{y,i}}{b_{y,i}}\right|$, according to Eqs. (3) and (6), Eq. (5) can be rewritten as follows:

$$\begin{aligned}
\dot{V}_1 &= \frac{y_{e,i}\dot{y}_{e,i}}{\cos^2\left(\frac{\pi {y_{e,i}}^2}{2b_{y,i}^2}\right)} + \frac{2b_{y,i}\dot{b}_{y,i}}{\pi}\tan\left(\frac{\pi {y_{e,i}}^2}{2b_{y,i}^2}\right) - \left(\frac{\dot{b}_{y,ic}}{b_{y,i}}\right)\frac{{y_{e,i}}^2}{\cos^2\left(\frac{\pi {y_{e,i}}^2}{2b_{y,i}^2}\right)} \\
&\leq \frac{y_{e,i}\dot{y}_{e,i}}{\cos^2\left(\frac{\pi {y_{e,i}}^2}{2b_{y,i}^2}\right)} - \left(\frac{\dot{b}_{y,ic}}{b_{y,i}}\right)\frac{{y_{e,i}}^2}{\cos^2\left(\frac{\pi {y_{e,i}}^2}{2b_{y,i}^2}\right)} + \frac{2k_b b_{y,i}^2}{\pi}\tan\left(\frac{\pi {y_{e,i}}^2}{2b_{y,i}^2}\right) \\
&\leq \frac{y_{e,i}v_i\sin\left(\theta_i - \theta_{p,i}\right)}{\cos^2\left(\frac{\pi {y_{e,i}}^2}{2b_{y,i}^2}\right)} - \left(\frac{\dot{b}_{y,ic}}{b_{y,i}}\right)\frac{{y_{e,i}}^2}{\cos^2\left(\frac{\pi {y_{e,i}}^2}{2b_{y,i}^2}\right)} + \frac{2k_b b_{y,i}^2}{\pi}\tan\left(\frac{\pi {y_{e,i}}^2}{2b_{y,i}^2}\right) \\
&\leq \frac{y_{e,i}\left(-\frac{k_d b_{y,i}^2}{2\pi y_{e,i}}\sin\left(\frac{\pi y_{e,i}^2}{b_{y,i}^2}\right) + \frac{\dot{b}_{y,i}}{b_{y,i}}y_{e,i}\right)}{\cos^2\left(\frac{\pi {y_{e,i}}^2}{2b_{y,i}}\right)} - \left(\frac{\dot{b}_{y,ic}}{b_{y,i}}\right)\frac{{y_{e,i}}^2}{\cos^2\left(\frac{\pi {y_{e,i}}^2}{2b_{y,i}^2}\right)} + \frac{2k_b b_{y,i}^2}{\pi}\tan\left(\frac{\pi {y_{e,i}}^2}{2b_{y,i}^2}\right) \\
&\leq -\left(k_d - 2k_b\right)\frac{b_{y,i}^2}{\pi}\tan\left(\frac{\pi {y_{e,i}}^2}{2b_{y,i}^2}\right)
\end{aligned} \tag{7}$$

By choosing $k_d > 2k_b$, the following inequality holds:

$$\dot{V}_1 \leq -c_1 V_1, \tag{8}$$

where $c_1 = k_d - 2k_b$.

From Figure 3, the derivative of $x_{e,i}$ can be obtained as follows:

$$\dot{x}_{e,i} = v_j - v_i\cos\beta_i. \tag{9}$$

A Lyapunov function is given as:

$$V_2 = \frac{b_{x,i}^2}{\pi}\tan\left(\frac{\pi {x_{e,i}}^2}{2b_{x,i}^2}\right). \tag{10}$$

Also, according to the guidance law, the desired velocity is designed as follows:

$$v_{d,i} = \frac{1}{\cos\beta_i}\left(\frac{k_v b_{x,i}^2}{2\pi x_{e,i}}\sin\left(\frac{\pi x_{e,i}^2}{b_{x,i}^2}\right) - \frac{\dot{b}_{x,i}}{b_{x,i}}x_{e,i} + v_j\right), \tag{11}$$

 doi:10.20944/preprints202402.1744.v1



where $\beta_i = \theta_{i,j,p} - \theta_i$.

Upon differentiating the equation provided in Eq. (10), the resulting expression for $\dot{V}_2$ is given by:

$$\begin{aligned}
\dot{V}_2 &= \frac{x_{e,i}\dot{x}_{e,i}}{\cos^2\left(\frac{\pi {x_{e,i}}^2}{2b_{x,i}^2}\right)} + \frac{2b_{x,i}\dot{b}_{x,i}}{\pi}\tan\left(\frac{\pi {x_{e,i}}^2}{2b_{x,i}^2}\right) - \left(\frac{\dot{b}_{x,ic}}{b_{x,i}}\right)\frac{{x_{e,i}}^2}{\cos^2\left(\frac{\pi {x_{e,i}}^2}{2b_{x,i}^2}\right)} \\
&\leq \frac{x_{e,i}\dot{x}_{e,i}}{\cos^2\left(\frac{\pi x_{e,i}^2}{2b_{x,i}^2}\right)} - \left(\frac{\dot{b}_{x,i}}{b_{x,i}}\right)\frac{x_{e,i}^2}{\cos^2\left(\frac{\pi x_{e,i}^2}{2b_{x,i}^2}\right)} + \frac{2k_c b_{x,i}^2}{\pi}\tan\left(\frac{\pi x_{e,i}^2}{2b_{x,i}^2}\right) \\
&\leq \frac{x_{e,i}\left(v_j - v_i\cos\beta_i\right)}{\cos^2\left(\frac{\pi x_{e,i}^2}{2b_{x,i}^2}\right)} - \left(\frac{\dot{b}_{x,i}}{b_{x,i}}\right)\frac{{x_{e,i}}^2}{\cos^2\left(\frac{\pi x_{e,i}^2}{2b_{x,i}^2}\right)} + \frac{2k_c b_{x,i}^2}{\pi}\tan\left(\frac{\pi x_{e,i}^2}{2b_{x,i}^2}\right) \\
&\leq -\left(k_v - 2k_c\right)\frac{b_{x,i}^2}{\pi}\tan\left(\frac{\pi x_{e,i}^2}{2b_{x,i}^2}\right)
\end{aligned} \tag{12}$$

where $k_c = \sup\left|\frac{\dot{b}_{x,i}}{b_{x,i}}\right|$.

By selecting $k_v > 2k_c$, we can additionally derive:

$$\dot{V}_2 \leq -c_2 V_2, \tag{13}$$

where $c_2 = k_v - 2k_c$.

### *3.2. Orientation Angle Controller Design*

Now, with the guidance law supplying the desired yaw angle and velocity, it is imperative to devise controllers for these parameters. The controllers are developed independently, providing various practical advantages, including modularity, specialization, simplicity, robustness, and scalability. For formation member $i$, defining the angle error as

$$e_{\theta,i} = \theta_i - \theta_{d,i} \tag{14}$$

the computations of the derivatives of $\theta_{d,i}$ are extremely intricate. To mitigate this complexity, we introduce a second-order filter expressed as:

$$\begin{cases} \dot{\Phi}_{10} = \Phi_{20} \\ \dot{\Phi}_{20} = -2\zeta_0\omega_{n0}\Phi_{20} - \omega_n^2\left(\Phi_{10} - \theta_{d,i}\right) \end{cases}. \tag{15}$$

Here, the damping rate $\zeta_0$ and frequency $\omega_{n0}$ are predetermined constants, $\theta_{d,i}$ represents the input, $\Phi_{10}$ is the output and an estimation of $\theta_{d,i}$, and $\Phi_{20}$ can be interpreted as the derivative of $\theta_{d,i}$, denoted as $\hat{\theta}_{d,i}$. The estimated error of this second-order filter is defined as follows:

$$\tilde{\theta}_{d,i} = \dot{\theta}_{d,i} - \hat{\theta}_{d,i}. \tag{16}$$

Consider a Lyapunov candidate

$$V_0 = \frac{1}{2}e_{\theta,i}^2 \tag{17}$$

 doi:10.20944/preprints202402.1744.v1



and refer to Eqs. (1) and (16). The derivative of $V_0$ with respect to time can be expressed as:

$$\begin{aligned}\dot{V}_0 &= e_{\theta,i}\dot{e}_{\theta,i} \\ &= e_{\theta,i}\left(\dot{\theta}_i - \dot{\theta}_{d,i}\right) \\ &= e_{\theta,i}\left(\sigma_i^{-1} v_i \tan\left(\delta_i\right) + f_{\theta,i} + d_{\theta,i} - \hat{\theta}_{d,i} - \tilde{\theta}_{d,i}\right).\end{aligned} \tag{18}$$

RBFNN stands for Radial Basis Function Neural Network, which is a type of artificial neural network that is commonly used for function approximation and pattern recognition tasks. It comprises three layers: an input layer, a hidden layer featuring radial basis functions, and an output layer. In this study, we employ an RBFNN to approximate unknown nonlinear functions. Consequently,

$$\begin{aligned}\dot{V}_0 &= e_{\theta,i}\left(\sigma_i^{-1} v_i \tan\left(\delta_i\right) + W_{\theta,i}\varphi_{\theta,i} + \varepsilon_{\theta,i} + d_{\theta,i} - \hat{\theta}_{d,i} - \tilde{\theta}_{d,i}\right) \\ &= e_{\theta,i}\left(\sigma_i^{-1} v_i \tan\left(\delta_i\right) + W_{\theta,i}\varphi_{\theta,i} - \hat{\theta}_{d,i} + \tilde{d}_{\theta,i}\right),\end{aligned} \tag{19}$$

where $\tilde{d}_{\theta,i} = \varepsilon_{\theta,i} + d_{\theta,i} - \tilde{\theta}_{d,i}$ represents total disturbances. It is evident that $\tilde{d}_{\theta,i}$ is bounded, adhering to $\tilde{d}_{\theta,i} \leq \bar{d}_{\theta,i}$. Furthermore, $\tilde{W}_{\theta,i} = W_{\theta,i} - \hat{W}_{\theta,i}$ and $W_{\theta,i} \leq \bar{W}_{\theta,i}$.

To deal with the unknown nonlinear functions, the adaptive law is designed as follows:

$$\dot{\hat{W}}_{\theta,i} = k_{1,\theta,i}\left(\varphi_{\theta,i} e_{\theta,i} - k_{2,\theta,i}\hat{W}_{\theta,i}\right) \tag{20}$$

with positive parameters $k_{1,\theta,i}$ and $k_{2,\theta,i}$.

To deal with nominal disturbance, another adaptive law is designed as follows:

$$\dot{\hat{d}}_{\theta,i} = k_{3,\theta,i}\left(e_{\theta,i} - k_{4,\theta,i}\hat{d}_{\theta,i}\right) \tag{21}$$

with positive parameters $k_{3,\theta,i}$ and $k_{4,\theta,i}$.

For the adaptive tracking controller, the intended steering angle of the front wheels can be formulated as follows:

$$\delta_{d,i} = \arctan\left(v_i^{-1}\sigma_i(-k_{5,\theta,i}e_{\theta,i} - \hat{d}_{\theta,i} - \hat{W}_{\theta,i}\varphi_{\theta,i} + \hat{\theta}_{d,i})\right). \tag{22}$$

Consider a Lyapunov candidate given by:

$$V_3 = \frac{1}{2}e_{\theta,i}^2 + \frac{1}{2}k_{3,\theta,i}^{-1}\hat{d}_{\theta,i}^2 + \frac{1}{2}k_{1,\theta,i}^{-1}\tilde{W}_{\theta,i}^2, \tag{23}$$

where $\tilde{d} = \bar{d} - \hat{d}$, and combine Eqs. (20), (32), and (35). We can express the time derivative of $V_3$ as follows:

$$\begin{aligned}\dot{V}_3 =& e_{\theta,i}\dot{e}_{\theta,i} + \hat{d}_{\theta,i}\dot{\hat{d}}_{\theta,i} + \tilde{W}_{\theta,i}\dot{\tilde{W}}_{\theta,i} \\ =& e_{\theta,i}\left(\sigma_i^{-1} v_i \tan\left(\delta_i\right) + W_{\theta,i}\varphi_{\theta,i} - \hat{\theta}_{d,i} + \tilde{d}_{\theta,i}\right) + \hat{d}_{\theta,i}\left(e_{\theta,i} - k_{4,\theta,i}\hat{d}_{\theta,i}\right) - \tilde{W}_{\theta,i}\dot{\hat{W}}_{\theta,i} \\ =& e_{\theta,i}\left(-k_{5,\theta,i}e_{\theta,i} - \hat{d}_{\theta,i} - \hat{W}_{\theta,i}\varphi_{\theta,i} + W_{\theta,i}\varphi_{\theta,i} + \tilde{d}_{\theta,i}\right) + \hat{d}_{\theta,i}\left(e_{\theta,i} - k_{4,\theta,i}\hat{d}_{\theta,i}\right) \\ & - \tilde{W}_{\theta,i}\left(\varphi_{\theta,i}e_{\theta,i} - k_{2,\theta,i}\hat{W}_{\theta,i}\right) \\ \leq& -k_{5,\theta,i}e_{\theta,i}^2 - k_{4,\theta,i}\hat{d}_{\theta,i}^2 + e_{\theta,i}\bar{d}_{\theta,i} + k_{2,\theta,i}\tilde{W}_{\theta,i}\hat{W}_{\theta,i} \\ \leq& -k_{5,\theta,i}e_{\theta,i}^2 - k_{4,\theta,i}\hat{d}_{\theta,i}^2 + e_{\theta,i}\bar{d}_{\theta,i} + k_{2,\theta,i}\left\|\tilde{W}_{\theta,i}\right\|\left\|\hat{W}_{\theta,i}\right\| \\ \leq& -k_{5,\theta,i}e_{\theta,i}^2 - k_{4,\theta,i}\hat{d}_{\theta,i}^2 + e_{\theta,i}\bar{d}_{\theta,i} + k_{2,\theta,i}\left\|\tilde{W}_{\theta,i}\right\|\left(\bar{W}_{\theta,i} - \left\|\tilde{W}_{\theta,i}\right\|\right)\end{aligned} \tag{24}$$

where $\|W_{\theta,i}\| \leq \bar{W}_{\theta,i}$.

 doi:10.20944/preprints202402.1744.v1



Utilizing Lemma 2, we can derive the following inequalities:

$$\left\|\tilde{W}_{\theta,i}\right\|\left(\bar{W}_{\theta,i}-\left\|\tilde{W}_{\theta,i}\right\|\right)\leq-\frac{1}{2}\left\|\tilde{W}_{\theta,i}\right\|^2+\frac{1}{2}\bar{W}_{\theta,i}^2 \tag{25}$$

and

$$e_{\theta,i}\bar{d}_{\theta,i}\leq\frac{1}{2}\|e_{\theta,i}\|^2+\frac{1}{2}\bar{d}_{\theta,i}^2. \tag{26}$$

Then, combining these inequalities, we obtain:

$$\begin{aligned}\dot{V}_3\leq&-k_{5,\theta,i}e_{\theta,i}^2-k_{4,\theta,i}\hat{d}_{\theta,i}^2-\frac{1}{2}k_{2,\theta,i}\left\|\tilde{W}_{\theta,i}\right\|^2+\frac{1}{2}\|e_{\theta,i}\|^2+\frac{1}{2}\bar{d}_{\theta,i}^2+k_{2,\theta,i}\frac{1}{2}\left\|\bar{W}_{\theta,i}\right\|^2\\\leq&-(k_{5,\theta,i}-\frac{1}{2})e_{\theta,i}^2-k_{4,\theta,i}\hat{d}_{\theta,i}^2-\frac{1}{2}k_{2,\theta,i}\left\|\tilde{W}_{\theta,i}\right\|^2+\frac{1}{2}\bar{d}_{\theta,i}^2+k_{2,\theta,i}\frac{1}{2}\left\|\bar{W}_{\theta,i}\right\|^2\end{aligned} \tag{27}$$

From this, we can conclude that $\dot{V}_3\leq-\sigma_3V_3+\zeta_1$ where $\sigma_3=\min\{k_{5,\theta,i}-\frac{1}{2},k_{4,\theta,i},k_{2,\theta,i}\}>0$ and $\zeta_1=\frac{1}{2}\bar{d}_{\theta,i}^2+k_{2,\theta,i}\frac{1}{2}\left\|\bar{W}_{\theta,i}\right\|^2>0$.

### *3.3. Velocity Controller Design*

For formation members, the velocity error is defined as:

$$e_{v,i}=v_i-v_{d,i} \tag{28}$$

The computations of the derivatives of $v_{d,i}$ are extremely intricate. Therefore, a second-order filter is introduced to solve this problem as

$$\begin{cases}\dot{\Phi}_{30}=\Phi_{40}\\\dot{\Phi}_{40}=-2\zeta_0\omega_{n0}\Phi_{40}-\omega_n^2\left(\Phi_{10}-v_{d,i}\right)\end{cases} \tag{29}$$

where damp rate $\zeta_0$ and frequency $\omega_{n0}$ are designed constants, $v_{d,i}$ is the input, $\Phi_{30}$ is the output and the estimation of $v_{d,i}$, $\Phi_{40}$ can be taken as the derivative of $v_{d,i}$ which is denoted as $\hat{v}_{d,i}$.

The estimate error of this second-order filter is defined as

$$\tilde{v}_{d,i}=\dot{v}_{d,i}-\hat{v}_{d,i} \tag{30}$$

Differentiating the velocity error,

$$\begin{aligned}\dot{e}_{v,i}&=\dot{v}_i-\dot{v}_{d,i}\\&=F_i+f_{v,i}(v_i)+d_{v,i}-\hat{v}_{d,i}-\tilde{v}_{d,i}\end{aligned} \tag{31}$$

In this paper, an RBFNN is employed to approximate unknown nonlinear functions. Then,

$$\begin{aligned}\dot{e}_{v,i}&=F_i+W_{v,i}\varphi_{v,i}+\varepsilon_{v,i}+d_{v,i}-\hat{v}_{d,i}-\tilde{v}_{d,i}\\&=F_i+W_{v,i}\varphi_{v,i}+d_{v,i}-\hat{v}_{d,i}+\tilde{d}_{v,i}\end{aligned} \tag{32}$$

where $\tilde{d}_{v,i}=\varepsilon_{v,i}+d_{v,i}-\tilde{v}_{d,i}$ is total disturbances. Apparently, $\tilde{d}_{v,i}$ is bounded, satisfying $\tilde{d}_{v,i}\leq\bar{d}_{v,i}$. $\tilde{W}_{v,i}=W_{v,i}-\hat{W}_{v,i}$ and $W_{v,i}\leq\bar{W}_{v,i}$.

To deal with the unknown nonlinear functions, the adaptive law is designed as

$$\dot{\hat{W}}_{v,i}=k_{1,v,i}\left(\varphi_{v,i}e_{v,i}-k_{2,v,i}\hat{W}_{v,i}\right) \tag{33}$$

with positive parameters $k_{1,v,i}$ and $k_{2,v,i}$.

 doi:10.20944/preprints202402.1744.v1



To deal with nominal disturbance, another adaptive law is designed as

$$\dot{\hat{d}}_{v,i} = k_{3,v,i}\left(e_{v,i} - k_{4,v,i}\hat{d}_{v,i}\right) \tag{34}$$

with positive parameters $k_{3,v,i}$ and $k_{4,v,i}$. The adaptive tracking controller for the desired velocity can be formulated as follows:

$$F_{d,i} = -k_{5,v,i}e_{v,i} - \hat{d}_{v,i} - \hat{W}_{v,i}\varphi_{v,i} + \hat{v}_{d,i}. \tag{35}$$

Consider a Lyapunov candidate

$$V_4 = \frac{1}{2}e_{v,i}^2 + \frac{1}{2}k_{3,v,i}^{-1}\hat{d}_{v,i}^2 + \frac{1}{2}k_{1,v,i}^{-1}\tilde{W}_{v,i}^2. \tag{36}$$

Then, by combining Eqs. (31), (34), and (33), we can describe the differential of $V_4$ as follows:

$$\begin{aligned}
\dot{V}_4 =& e_{v,i}\dot{e}_{v,i} + \hat{d}_{v,i}\dot{\hat{d}}_{v,i} + \tilde{W}_{v,i}\dot{\hat{W}}_{v,i} \\
=& e_{v,i}\left(F_i + W_{v,i}\varphi_{v,i} - \hat{v}_{d,i} + \tilde{d}_{v,i}\right) + \hat{d}_{v,i}\left(e_{v,i} - k_{4,v,i}\hat{d}_{v,i}\right) - \tilde{W}_{v,i}\dot{\hat{W}}_{v,i} \\
=& e_{v,i}\left(-k_{5,v,i}e_{v,i} - \hat{d}_{v,i} - \hat{W}_{v,i}\varphi_{v,i} + W_{v,i}\varphi_{v,i} + \tilde{d}_{v,i}\right) + \hat{d}_{v,i}\left(e_{v,i} - k_{4,v,i}\hat{d}_{v,i}\right) \\
& - \tilde{W}_{v,i}\left(\varphi_{v,i}e_{v,i} - k_{2,v,i}\hat{W}_{v,i}\right) \\
\leq& -k_{5,v,i}e_{v,i}^2 - k_{4,v,i}\hat{d}_{v,i}^2 + e_{v,i}\bar{d}_{v,i} + k_{2,v,i}\tilde{W}_{v,i}\hat{W}_{v,i} \\
\leq& -k_{5,v,i}e_{v,i}^2 - k_{4,v,i}\hat{d}_{v,i}^2 + e_{v,i}\bar{d}_{v,i} + k_{2,v,i}\left\|\tilde{W}_{v,i}\right\|\left\|\hat{W}_{v,i}\right\| \\
\leq& -k_{5,v,i}e_{v,i}^2 - k_{4,v,i}\hat{d}_{v,i}^2 + e_{v,i}\bar{d}_{v,i} + k_{2,v,i}\left\|\tilde{W}_{v,i}\right\|\left(\bar{W}_{v,i} - \left\|\tilde{W}_{v,i}\right\|\right)
\end{aligned} \tag{37}$$

where $\|W_{v,i}\| \leq \bar{W}_{v,i}$.

Utilizing Lemma 2, we can derive the following inequalities:

$$\left\|\tilde{W}_{v,i}\right\|\left(\bar{W}_{v,i} - \left\|\tilde{W}_{v,i}\right\|\right) \leq -\frac{1}{2}\left\|\tilde{W}_{v,i}\right\|^2 + \frac{1}{2}\bar{W}_{v,i}^2 \tag{38}$$

and

$$e_{v,i}\bar{d}_{v,i} \leq \frac{1}{2}\|e_{v,i}\|^2 + \frac{1}{2}\bar{d}_{v,i}^2. \tag{39}$$

Combining these inequalities, we obtain:

$$\begin{aligned}
\dot{V}_4 \leq& -k_{5,v,i}e_{v,i}^2 - k_{4,v,i}\hat{d}_{v,i}^2 - \frac{1}{2}k_{2,v,i}\left\|\tilde{W}_{v,i}\right\|^2 + \frac{1}{2}\|e_{v,i}\|^2 + \frac{1}{2}\bar{d}_{v,i}^2 \\
& + k_{2,v,i}\frac{1}{2}\left\|\bar{W}_{v,i}\right\|^2 \\
\leq& -(k_{5,v,i} - \frac{1}{2})e_{v,i}^2 - k_{4,v,i}\hat{d}_{v,i}^2 - \frac{1}{2}k_{2,v,i}\left\|\tilde{W}_{v,i}\right\|^2 \\
& + \frac{1}{2}\bar{d}_{v,i}^2 + k_{2,v,i}\frac{1}{2}\left\|\bar{W}_{v,i}\right\|^2.
\end{aligned} \tag{40}$$

The conclusion can be given that $\dot{V}_4 \leq -\sigma_4 V_4 + \zeta_2$ with

$$\sigma_4 = \min\{k_{5,v,i} - \frac{1}{2}, k_{4,v,i}, k_{2,v,i}\} > 0 \tag{41}$$

and

$$\zeta_2 = \frac{1}{2}\bar{d}_{v,i}^2 + k_{2,v,i}\frac{1}{2}\left\|\bar{W}_{v,i}\right\|^2 > 0. \tag{42}$$

 doi:10.20944/preprints202402.1744.v1



### 3.4. Stability Analysis

Consider the Lyapunov candidate represented as:

$$\begin{aligned} V =& V_1 + V_2 + V_3 + V_4 \\ =& \frac{b_{x,i}^2}{\pi} \tan\left(\frac{\pi {x_{e,i}}^2}{2b_{x,i}^2}\right) + \frac{b_{y,i}^2}{\pi} \tan\left(\frac{\pi {y_{e,i}}^2}{2b_{y,i}^2}\right) + \frac{1}{2}e_{\theta,i}^2 + \frac{1}{2}k_{3,\theta,i}^{-1}\hat{d}_{\theta,i}^2 + \frac{1}{2}k_{1,\theta,i}^{-1}\tilde{W}_{\theta,i}^2 \\ &+ \frac{1}{2}e_{v,i}^2 + \frac{1}{2}k_{3,v,i}^{-1}\hat{d}_{v,i}^2 + \frac{1}{2}k_{1,v,i}^{-1}\tilde{W}_{v,i}^2 \end{aligned} \tag{43}$$

It concludes that $\dot{V} \leq -\sigma V + \zeta$ in which

$$\sigma = \min\left\{k_d - 2k_b, k_v - 2k_c, k_{5,\theta,i} - \frac{1}{2}, k_{4,\theta,i}, k_{2,\theta,i}, k_{5,v,i} - \frac{1}{2}, k_{4,v,i}, k_{2,v,i}\right\} > 0 \tag{44}$$

and

$$\zeta = \frac{1}{2}\bar{d}_{v,i}^2 + k_{2,v,i}\frac{1}{2}\left\|\bar{W}_{v,i}\right\|^2 + \frac{1}{2}\bar{d}_{\theta,i}^2 + k_{2,\theta,i}\frac{1}{2}\left\|\bar{W}_{\theta,i}\right\|^2 > 0. \tag{45}$$

Choosing parameters such that $k_d > 2k_b$, $k_v > 2k_c$, $k_{5,\theta,i} > \frac{1}{2}$, and $k_{5,v,i} > \frac{1}{2}$, and integrating Eq. (43), we can derive the inequality $V \leq \left(V(0) - \frac{\zeta}{\sigma}\right)e^{-\sigma t} + \frac{\zeta}{\sigma}$. The conclusion can be drawn that $V$ is bounded. Moreover, $\frac{b_{x,i}^2}{\pi}\tan\left(\frac{\pi {x_{e,i}}^2}{2b_{x,i}^2}\right) \leq V \leq \left(V(0) - \frac{\zeta}{\sigma}\right)e^{-\sigma t} + \frac{\zeta}{\sigma}$ and $\frac{b_{y,i}^2}{\pi}\tan\left(\frac{\pi {y_{e,i}}^2}{2b_{y,i}^2}\right) \leq V \leq \left(V(0) - \frac{\zeta}{\sigma}\right)e^{-\sigma t} + \frac{\zeta}{\sigma}$ imply the following constraints hold:

$${x_{e,i}}^2 \leq \frac{2b_{x,i}^2}{\pi}\tan^{-1}\left(\frac{\pi}{b_{x,i}^2}\left(\left(V(0) - \frac{\zeta}{\sigma}\right)e^{-\sigma t} + \frac{\zeta}{\sigma}\right)\right) < b_{x,i}^2 \tag{46}$$

and

$${y_{e,i}}^2 \leq \frac{2b_{y,i}^2}{\pi}\tan^{-1}\left(\frac{\pi}{b_{y,i}^2}\left(\left(V(0) - \frac{\zeta}{\sigma}\right)e^{-\sigma t} + \frac{\zeta}{\sigma}\right)\right) < b_{y,i}^2 \tag{47}$$

Therefore, the conclusion can be drawn that $x_{e,i}$ and $y_{e,i}$ are bounded as $|x_{e,i}| < |b_{x,i}|$ and $|y_{e,i}| < |b_{y,i}|$. Finally, theses terms can be eliminated to a small neighborhood around zero.

## 4. Simulation Result

In this Section, the simulation results of the formation control with different disturbances are shown. In our simulation, Vehicle 1 serves as the leader, with Vehicles 2, 3, and 4 acting as followers. The leader's desired trajectory, denoted as $(x_1(t), y_1(t))$, follows the equations $x_1(t) = 0.5 + 5e^{-0.2t}$ and $y_1(t) = 0.5 + 5e^{-0.2t}$. The vehicles are configured in a quadrilateral formation, with each diagonal measuring 20 meters. Initially, Vehicle 2 is positioned at $(-5.5, -9.9)$, Vehicle 3 at $(-6.5, 10)$, and Vehicle 4 at $(-18.5, 0.1)$. All vehicles maintain a constant velocity of 1 $m/s$ throughout the simulation.

 doi:10.20944/preprints202402.1744.v1



**Table 1.** Main parameters of the controller.

| Parameter | Value | Parameter | Value |
|---|---|---|---|
| $k_y$ | 1.01 | $k_{4,\theta,i}$ | 1.01 |
| $k_v$ | 1.1 | $k_{5,\theta,i}$ | 2 |
| $k_{1,\theta,i}$ | 0.5 | $k_{3,v,i}$ | 1 |
| $k_{2,\theta,i}$ | 8 | $k_{4,v,i}$ | 1 |
| $k_{1,v,i}$ | 5 | $k_{5,v,i}$ | 0.2 |
| $k_{2,v,i}$ | 18 | $\zeta_0$ | 0.8 |
| $k_{3,\theta,i}$ | 5 | $\omega_{n0}$ | 20 |

Figure 5 depicts the trajectory of the formation, which maintains its predefined shape effectively even in the presence of various disturbances. The simulation results in Figure 4 and 6 provide a comprehensive analysis of the formation control algorithm's capability to minimize trajectory tracking errors for the followers.

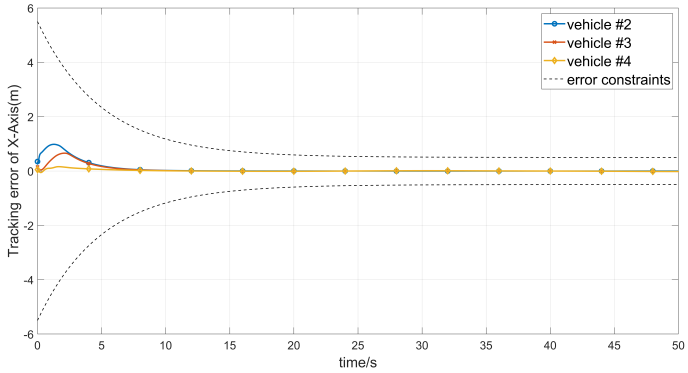


(a)

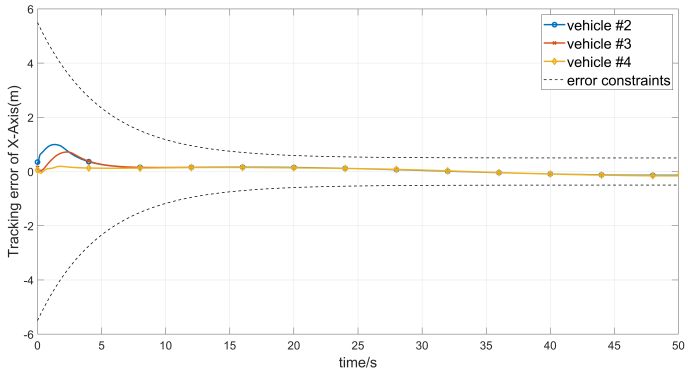


(b)

**Figure 4.** Trajectory tracking error of x-axis with different disturbances:**(a)** Without disturb, **(b)** $d_{\theta,i}(t)$, $d_{v,i}(t) = 0.5 \sin \frac{t}{10}$

 doi:10.20944/preprints202402.1744.v1



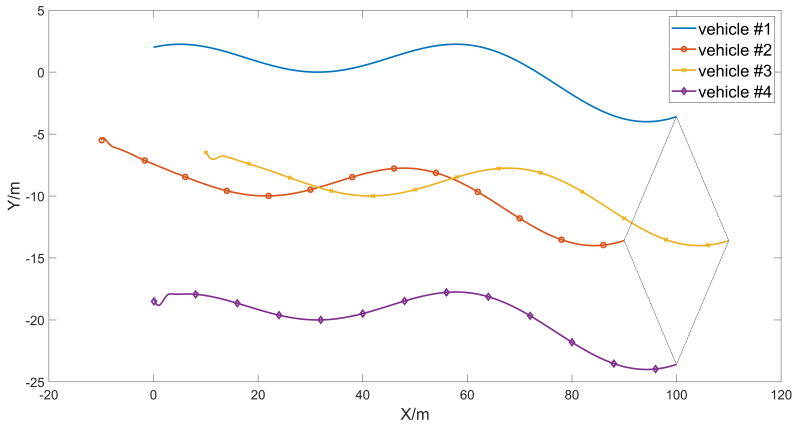


(a)

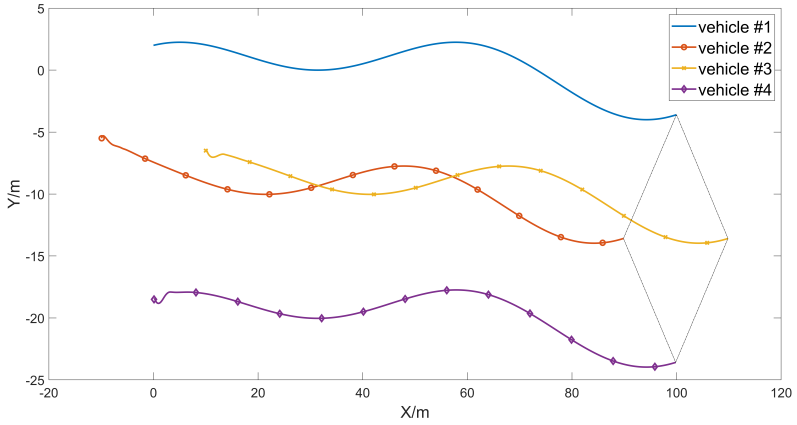


(b)

**Figure 5.** Trajectory of formation with different disturbances:**(a)** Without disturb and **(b)** $d_{\theta,i}(t)$, $d_{v,i}(t)$ $= 0.5 \sin \frac{t}{10}$

Initially, at the beginning of the simulation, the position errors along the x and y axes for the followers are approximately 1m, which can be attributed to random initial conditions. However, as the simulation progresses, the formation control algorithm effectively guides the followers towards their target positions, leading to a rapid convergence of position errors. Within a short period, the errors decreased significantly, demonstrating the high precision and effectiveness achieved by the control strategy.

The figures also showcase the error constraints, which define the acceptable range of position errors during operation $(0.5m)$. The trajectory tracking error consistently stays well within the specified constraints throughout the simulation, affirming the robustness and effectiveness of the proposed formation control algorithm in managing the agents' motion while adhering to predefined error boundaries.

 doi:10.20944/preprints202402.1744.v1



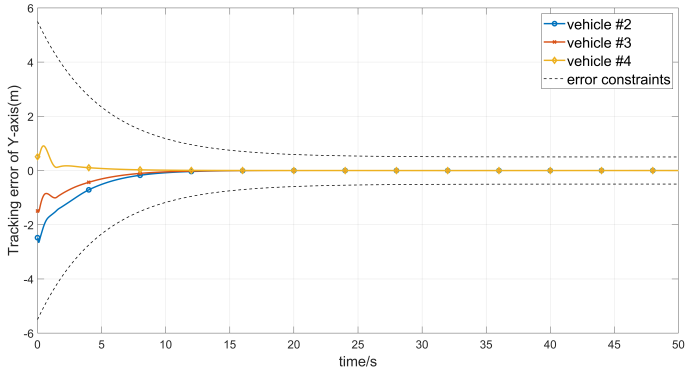


(a)

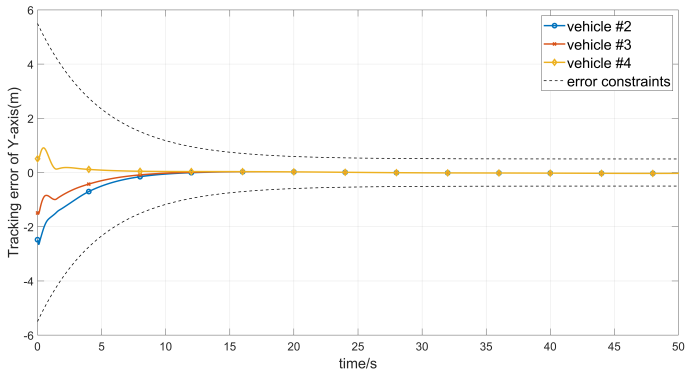


(b)

**Figure 6.** Trajectory tracking error of y-axis with different disturbances:**(a)** Without disturb, and **(b)** $d_{\theta,i}(t), d_{v,i}(t) = 0.5 \sin \frac{t}{10}$

As depicted in Figure 7, the leader's angular change exhibits a smooth transition, aligning well with real-world applications. In the initial startup phase (approximately the first 2 seconds), the three followers swiftly adjust their angles within a range of 55 to 140 degrees. Subsequently, they converge to a narrower variation range of 90 to 100 degrees. Around the 5-second mark, Vehicle 4's angle closely aligns with the leader's angle, maintaining this alignment throughout the simulation. Similarly, Vehicles 2 and 3 achieve alignment with the leader around the 12-second mark, displaying no visible deviation for the remainder of the simulation. This highlights the efficacy of the formation control algorithm in synchronizing the followers' angular changes with the leader's smooth trajectory.

 doi:10.20944/preprints202402.1744.v1



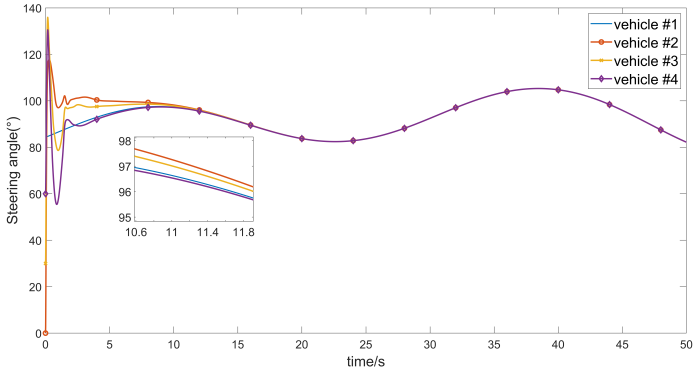


(a)

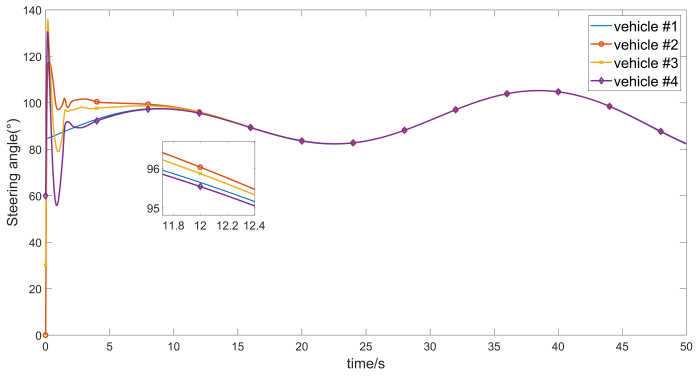


(b)

**Figure 7.** Steering angle error of formation with different disturbances: **(a)** Without disturb and **(b)** $d_{\theta,i}(t), d_{v,i}(t) = 0.5 \sin \frac{t}{10}$

The velocity progression of the formation members is illustrated in Figure 8. Within the initial 3 seconds, Vehicles 2, 3, and 4 rapidly converge their speeds to a range of $1.8 - 2.5$ m/s and subsequently maintain a speed almost consistent with that of Vehicle 1. Notably, the convergence speed of Vehicles 2 and 3 is significantly faster than that of Vehicle 4. This difference can be attributed to the varying initial positions of the vehicles. The observed behavior indirectly underscores that the proposed method in this study enables the vehicles to swiftly identify their positions and uphold the desired formation alongside the rest of the fleet.

 doi:10.20944/preprints202402.1744.v1



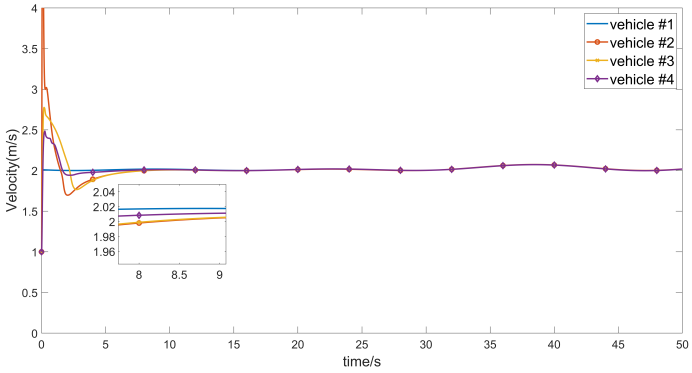


(a)

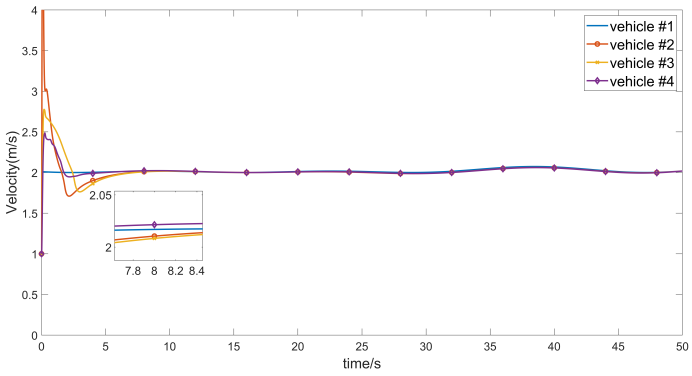


(b)

**Figure 8.** Vehicle velocity with different disturbances: **(a)** Without disturb and **(b)** $d_{\theta,i}(t)$, $d_{v,i}(t) = 0.5 \sin \frac{t}{10}$

Figures 9–fig:controlinput3 depict the control inputs applied to the followers under various disturbances. The inputs rapidly converge, demonstrating the stability of our approach.

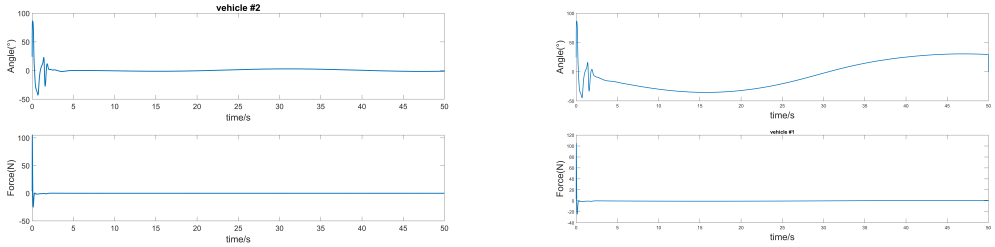


(a) (b)

**Figure 9.** Control inputs of follower1 with different disturbances:**(a)** Without disturb, **(b)** $d_{\theta,i}(t)$, $d_{v,i}(t) = 0.5 \sin \frac{t}{10}$

Preprints.org (www.preprints.org) | NOT PEER-REVIEWED | Posted: 29 February 2024 doi:10.20944/preprints202402.1744.v1



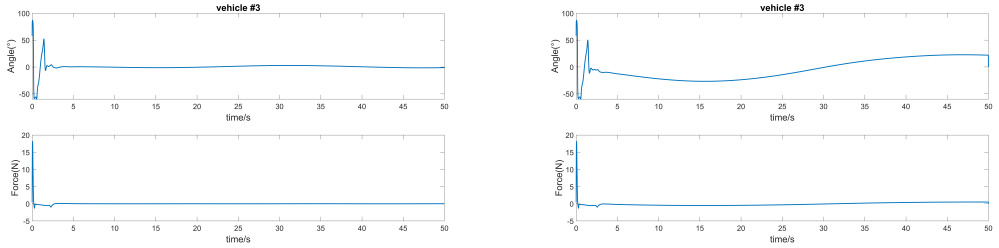


(a) (b)

**Figure 10.** Control inputs of follower2 with different disturbances:**(a)** Without disturb, **(b)** $d_{\theta,i}(t)$, $d_{v,i}(t) = 0.5 \sin \frac{t}{10}$

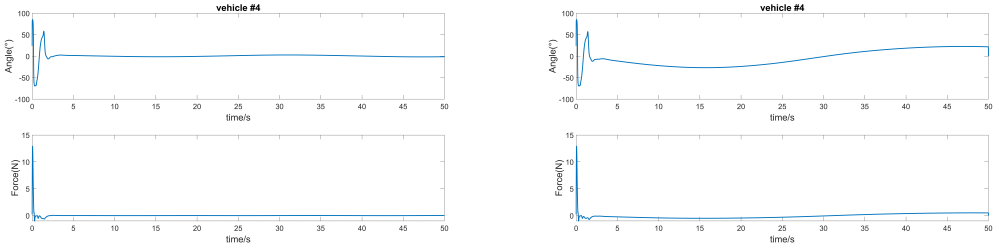


(a) (b)

**Figure 11.** Control inputs of follower3 with different disturbances:**(a)** Without disturb, **(b)** $d_{\theta,i}(t)$, $d_{v,i}(t) = 0.5 \sin \frac{t}{10}$

To provide a more detailed depiction of the results, we present the mean and maximum position errors of the followers in Tables 2–3. The tabulated outcomes clearly demonstrate the outstanding performance of the controller, consistent with our expectations.

**Table 2.** The mean and maximal position error of follower 1

| Disturbances | Mean position error (m) | Maximal position error (m) |
|---|---|---|
| $d_{\theta,1}(t), d_{v,1}(t) = 0$ | 0.1751 | 2.6776 |
| $d_{\theta,1}(t), d_{v,1}(t) = 0.5 \sin \frac{t}{10}$ | 0.2542 | 2.6838 |

**Table 3.** The mean and maximal position error of follower 2

| Disturbances | Mean position error (m) | Maximal position error (m) |
|---|---|---|
| $d_{\theta,2}(t), d_{v,2}(t) = 0$ | 0.1129 | 1.5380 |
| $d_{\theta,2}(t), d_{v,2}(t) = 0.5 \sin \frac{t}{10}$ | 0.1960 | 1.5377 |

**Table 4.** The mean and maximal position error of follower 3

| Disturbances | Mean position error (m) | Maximal position error (m) |
|---|---|---|
| $d_{\theta,3}(t), d_{v,3}(t) = 0$ | 0.0408 | 0.9130 |
| $d_{\theta,3}(t), d_{v,3}(t) = 0.5 \sin \frac{t}{10}$ | 0.1323 | 0.9096 |

## 5. Conclusion

This paper introduces an adaptive leader-follower formation controller with prescribed performance. The guidance law computes the desired velocity and steering angle based on the leader's trajectory and a predefined formation pattern. To address challenges posed by unknown functions and external disturbances, a second-order filter and an RBFNN, alongside an adaptive law,

are employed. Notably, the entire controller adheres to a backstepping method, incorporating distinct velocity and corner controllers to enhance system robustness. Furthermore, the inclusion of a barrier to the Lyapunov function contributes to achieving the prescribed performance. Simulation results illustrate that our proposed controller consistently attains superior performance within the specified limits, even in the presence of various disturbances.

**Author Contributions:** Conceptualization, F. X. and G. L.; methodology, F. X.; software, F. X.; validation, Y.-R.C., F. X. and G. L.; formal analysis, Y.-R.C., F. X. and G. L.; investigation, F. X.; resources, Y.-R.C. and F. X.; data curation, F. X. and G. L.; supervision, Y.-R.C.; writing—original draft preparation, Y.-R.C., F. X. and G. L.; writing—review and editing, Y.-R.C. and F. X.; project administration, Y.-R.C.; funding acquisition, Y.-R.C..

**Funding:** This work was supported in part by the Ministry of Science and Technology of Taiwan under Grant 112-2221-E-197-022.

**Data Availability Statement:** The article includes all the data supporting the results, and there is no need for any extra source data.

**Acknowledgments:** We would like to thank all the reviewers for their constructive comments.

**Conflicts of Interest:** The authors declare no conflict of interest.

## References

1. Balch, T.; Arkin, R. Behavior-based formation control for multirobot teams. *IEEE Transactions on Robotics and Automation* **1998**, *14*, 926–939. doi:10.1109/70.736776.
2. Do, K. Formation control of multiple elliptical agents with limited sensing ranges. *Automatica* **2012**, *48*, 1330–1338. doi:https://doi.org/10.1016/j.automatica.2012.04.005.
3. Li, X.; Pei, G.; Liu, L.; Chen, L.; Zhang, W. Metabolomic analysis and lipid accumulation in a glucose tolerant Crypthecodinium cohnii strain obtained by adaptive laboratory evolution. *Bioresource Technology* **2017**, *235*, 87–95. doi:https://doi.org/10.1016/j.biortech.2017.03.049.
4. Cao, Y.; Yu, W.; Ren, W.; Chen, G. An Overview of Recent Progress in the Study of Distributed Multi-Agent Coordination. *IEEE Transactions on Industrial Informatics* **2013**, *9*, 427–438.
5. Yuan, C.; He, H.; Wang, C. Cooperative Deterministic Learning-Based Formation Control for a Group of Nonlinear Uncertain Mechanical Systems. *IEEE Transactions on Industrial Informatics* **2019**, *15*, 319–333. doi:10.1109/TII.2018.2792455.
6. He, S.; Wang, M.; Dai, S.L.; Luo, F. Leader–Follower Formation Control of USVs With Prescribed Performance and Collision Avoidance. *IEEE Transactions on Industrial Informatics* **2019**, *15*, 572–581. doi:10.1109/TII.2018.2839739.
7. Yang, E.; Gu, D. Nonlinear Formation-Keeping and Mooring Control of Multiple Autonomous Underwater Vehicles. *IEEE/ASME Transactions on Mechatronics* **2007**, *12*, 164–178. doi:10.1109/TMECH.2007.892826.
8. Breivik, M.; Hovstein, V.E.; Fossen, T.I. Ship Formation Control: A Guided Leader-Follower Approach. *IFAC Proceedings Volumes* **2008**, *41*, 16008–16014. 17th IFAC World Congress, doi:https://doi.org/10.3182/20080706-5-KR-1001.02706.
9. Millán, P.; Orihuela, L.; Jurado, I.; Rubio, F.R. Formation Control of Autonomous Underwater Vehicles Subject to Communication Delays. *IEEE Transactions on Control Systems Technology* **2014**, *22*, 770–777. doi:10.1109/TCST.2013.2262768.
10. Yan, Z.; Yang, Z.; Yue, L.; Wang, L.; Jia, H.; Zhou, J. Discrete-time coordinated control of leader-following multiple AUVs under switching topologies and communication delays. *Ocean Engineering* **2019**, *172*, 361–372. doi:https://doi.org/10.1016/j.oceaneng.2018.12.018.
11. Zhang, L.; Tao, R.; Zhang, Z.X.; Chien, Y.R.; Bai, J. PMSM non-singular fast terminal sliding mode control with disturbance compensation. *Information Sciences* **2023**, *642*, 119040. doi:https://doi.org/10.1016/j.ins.2023.119040.
12. Wu, H.M.; Karkoub, M.; Hwang, C.L. Mixed Fuzzy Sliding-Mode Tracking with Backstepping Formation Control for Multi-Nonholonomic Mobile Robots Subject to Uncertainties. *Journal of Intelligent & Robotic Systems* **2015**, *79*, 73–86. doi:10.1007/s10846-014-0131-9.

13. Wang, J.; Wang, C.; Wei, Y.; Zhang, C. Neuroadaptive Sliding Mode Formation Control of Autonomous Underwater Vehicles With Uncertain Dynamics. *IEEE Systems Journal* **2020**, *14*, 3325–3333. doi:10.1109/JSYST.2019.2938315.
14. Zhang, L.; Bai, J.; Wu, J. Speed Sensor-Less Control System of Surface-Mounted Permanent Magnet Synchronous Motor Based on Adaptive Feedback Gain Supertwisting Sliding Mode Observer. *Journal of Sensors* **2021**, *2021*, 8301359. doi:10.1155/2021/8301359.
15. Su, B.; bin Wang, H.; Wang, Y. Dynamic event-triggered formation control for AUVs with fixed-time integral sliding mode disturbance observer. *Ocean Engineering* **2021**, *240*, 109893. doi:https://doi.org/10.1016/j.oceaneng.2021.109893.
16. Zhang, L.; Wang, S.; Bai, J. Fast-super-twisting sliding mode speed loop control of permanent magnet synchronous motor based on SVM-DTC. *IEICE Electron. Express* **2020**, *18*, 20200375.
17. Rout, R.; Subudhi, B. A backstepping approach for the formation control of multiple autonomous underwater vehicles using a leader–follower strategy. *Journal of Marine Engineering & Technology* **2016**, *15*, 38–46. doi:10.1080/20464177.2016.1173268.
18. Pang, S.; Wang, J.; Liu, J.; Yi, H. Three-dimensional leader–follower formation control of multiple autonomous underwater vehicles based on line-of-sight measurements using the backstepping method. *Proceedings of the Institution of Mechanical Engineers, Part I: Journal of Systems and Control Engineering* **2018**, *232*, 819–829. doi:10.1177/0959651818760936.
19. Chengmei Mu, Xinjiang Wei, H.Z.X.H.; Han, J. Disturbance observer-based backstepping control for leader–follower ships with disturbances. *Ships and Offshore Structures* **2023**, *0*, 1–9. doi:10.1080/17445302.2023.2186289.
20. Wang, F.; Gao, Y.; Zhou, C.; Zong, Q. Disturbance observer-based backstepping formation control of multiple quadrotors with asymmetric output error constraints. *Applied Mathematics and Computation* **2022**, *415*, 126693. doi:https://doi.org/10.1016/j.amc.2021.126693.
21. Zaidi, A.; Kazim, M.; Wang, H. A Robust Backstepping Sliding Mode Controller with Chattering-Free Strategy for a Swarm of Drones. *Journal of Physics: Conference Series* **2022**, *2213*, 012007. doi:10.1088/1742-6596/2213/1/012007.
22. Yang, K.; Dong, W.; Tong, Y.; He, L. Leader-follower Formation Consensus of Quadrotor UAVs Based on Prescribed Performance Adaptive Constrained Backstepping Control. *International Journal of Control, Automation and Systems* **2022**, *20*, 3138–3154. doi:10.1007/s12555-021-0437-x.
23. Shojaei, K. Neural adaptive PID formation control of car-like mobile robots without velocity measurements. *Advanced Robotics* **2017**, *31*, 947–964. doi:10.1080/01691864.2017.1368413.
24. Jia, Z.; Wang, L.; Yu, J.; Ai, X. Distributed adaptive neural networks leader-following formation control for quadrotors with directed switching topologies. *ISA Transactions* **2019**, *93*, 93–107. doi:https://doi.org/10.1016/j.isatra.2019.02.030.
25. Kuo, C.W.; Tsai, C.C.; Lee, C.T. Intelligent Leader-Following Consensus Formation Control Using Recurrent Neural Networks for Small-Size Unmanned Helicopters. *IEEE Transactions on Systems, Man, and Cybernetics: Systems* **2021**, *51*, 1288–1301. doi:10.1109/TSMC.2019.2896958.
26. Huang, C.; Zhang, X.; Zhang, G. Adaptive neural finite-time formation control for multiple underactuated vessels with actuator faults. *Ocean Engineering* **2021**, *222*, 108556. doi:https://doi.org/10.1016/j.oceaneng.2020.108556.
27. Rani, M.; Kumar, N. A neural network based efficient leader–follower formation control approach for multiple autonomous underwater vehicles. *Eng. Appl. Artif. Intell.* **2023**, *122*. doi:10.1016/j.engappai.2023.106102.
28. Zhao, X.; Chen, S.; Zhang, Z.; Zheng, Y. Consensus Tracking for High-Order Uncertain Nonlinear MASs via Adaptive Backstepping Approach. *IEEE Transactions on Cybernetics* **2023**, *53*, 1248–1259. doi:10.1109/TCYB.2021.3118782.
29. Huang, H.; Gong, M.; Zhuang, Y.; Sharma, S.; Xu, D. A new guidance law for trajectory tracking of an underactuated unmanned surface vehicle with parameter perturbations. *Ocean Engineering* **2019**, *175*, 217–222. doi:https://doi.org/10.1016/j.oceaneng.2019.02.042.
30. Xia, Y.; Xu, K.; Li, Y.; Xu, G.; Xiang, X. Improved line-of-sight trajectory tracking control of under-actuated AUV subjects to ocean currents and input saturation. *Ocean Engineering* **2019**, *174*, 14–30. doi:https://doi.org/10.1016/j.oceaneng.2019.01.025.

31. Rout, R.; Cui, R.; Han, Z. Modified Line-of-Sight Guidance Law With Adaptive Neural Network Control of Underactuated Marine Vehicles With State and Input Constraints. *IEEE Transactions on Control Systems Technology* **2020**, *28*, 1902–1914. doi:10.1109/TCST.2020.2998798.
32. Bechlioulis, C.P.; Rovithakis, G.A. Robust Adaptive Control of Feedback Linearizable MIMO Nonlinear Systems With Prescribed Performance. *IEEE Transactions on Automatic Control* **2008**, *53*, 2090–2099.
33. Wang, M.; Yang, A. Dynamic Learning From Adaptive Neural Control of Robot Manipulators With Prescribed Performance. *IEEE Transactions on Systems, Man, and Cybernetics: Systems* **2017**, *47*, 2244–2255. doi:10.1109/TSMC.2016.2645942.
34. Dai, S.L.; He, S.; Chen, X.; Jin, X. Adaptive Leader–Follower Formation Control of Nonholonomic Mobile Robots With Prescribed Transient and Steady-State Performance. *IEEE Transactions on Industrial Informatics* **2020**, *16*, 3662–3671. doi:10.1109/TII.2019.2939263.
35. Jiang, Y.; Liu, Z.; Chen, Z. Prescribed-time distributed formation control for a class of nonlinear multi-agent systems subject to internal uncertainties and external disturbances. *Nonlinear Dynamics* **2023**, *111*, 1643–1655. doi:10.1007/s11071-022-07909-2.
36. Dai, S.L.; He, S.; Cai, H.; Yang, C. Adaptive Leader–Follower Formation Control of Underactuated Surface Vehicles With Guaranteed Performance. *IEEE Transactions on Systems, Man, and Cybernetics: Systems* **2022**, *52*, 1997–2008. doi:10.1109/TSMC.2020.3036120.
37. Mehdifar, F.; Bechlioulis, C.P.; Hashemzadeh, F.; Baradarannia, M. Prescribed performance distance-based formation control of Multi-Agent Systems. *Automatica* **2020**, *119*, 109086. doi:https://doi.org/10.1016/j.automatica.2020.109086.
38. Verginis, C.K.; Bechlioulis, C.P.; Dimarogonas, D.V.; Kyriakopoulos, K.J. Robust Distributed Control Protocols for Large Vehicular Platoons With Prescribed Transient and Steady-State Performance. *IEEE Transactions on Control Systems Technology* **2018**, *26*, 299–304. doi:10.1109/TCST.2017.2658180.
39. Fan, B.; Yang, Q.; Jagannathan, S.; Sun, Y. Output-Constrained Control of Nonaffine Multiagent Systems With Partially Unknown Control Directions. *IEEE Transactions on Automatic Control* **2019**, *64*, 3936–3942. doi:10.1109/TAC.2019.2892391.